Electronic Supplementary Information (ESI) for Chemical Communications
This journal is (c) The Royal Society of Chemistry 2021

# Supporting Information

## MOFs-derived ruthenium-doped amorphous molybdenum dioxide hybrid for highly efficient hydrogen evolution reaction in alkaline media

Ji-Yuan Han,[a] Sheng-Hao Cai,[a] Shuang Yang,[a] Ji-Yu Zhu,[a] and Ji-Sen Li*,[a]

[a]Department of Chemistry and Chemical Engineering, Jining University, Qufu 273155, P. R. China.

E-mail: senjili@sina.com

## Experimental Section

### Materials

Copper acetate monohydrate ($Cu(OAc)_2 \cdot H_2O$), phosphomolybdic acid ($H_3PMo_{12}O_{40} \cdot nH_2O$), ruthenium chloride hydrate ($RuCl_3 \cdot xH_2O$), 1,3,5-benzenetricarboxylic acid ($H_3BTC$, 98%), sodium hydroxide (NaOH), and iron (III) chloride hexahydrate ($FeCl_3 \cdot 6H_2O$) were obtained from Sinopharm Chemical Reagent Co. Ltd. Commercial Pt/C (20 wt%) was provided by Johnson Matthey. Graphene oxide (GO) was purchased from XFNANO, China. All reagents were utilized without further purification.

**Preparation of NENU-5/GO**. Different amounts of GO (10, 20, and 40 mg) were dispersed into 10 mL of distilled water by ultrasonication for 2 h, respectively. Then, 0.2 g of $Cu(OAc)_2 \cdot H_2O$ and 0.17 g of $H_3PMo_{12}O_{40} \cdot nH_2O$ were added into the above solution and stirred for 30 min to form solution A. The pH of A was changed into 4.0 with the assistance of NaOH. 0.14 g of $H_3BTC$ was dissolved in ethanol solution (40 mL) to form solution B, which was added into the solution A with vigorously stirring. Finally, the product was collected, washed with alcohol/water, and dried at 50 $^oC$ for 12 h, which were denoted as NENU-5/GO (10, 20, and 40 mg), respectively.

In control experiment, NENU-5 was prepared with the identical method except for the addition of GO.

**Preparation of $RuCl_3$-NENU-5/GO**. In a typical procedure, 0.1 g of the resulting NENU-5/GO (10, 20, and 40 mg) were dispersed into 80 mL of the mixed solution ($V_{ethanol}$ : $V_{water}$ = 1:1) to achieve a uniform suspension, respectively, and then 60 μL of $RuCl_3 \cdot xH_2O$ solution (10 mg $mL^{-1}$) was added the above solution. After continuous stirring for 12 h, the products were filtered, washed with water and dried at 50 $^oC$, which were defined as $RuCl_3$-NENU-5/GO (10, 20, and 40 mg), respectively.

For comparison, $RuCl_3$-NENU-5 was also synthesized *via* the same processes for $RuCl_3$-NENU-5/GO.

**Preparation of Ru-$MoO_2$@PC/rGO**. The resultant $RuCl_3$-NENU-5/GO (20 mg) was carbonized at 600 $^oC$ under Ar for 5 h, and then etched by $FeCl_3$ solution (0.1 M) for 12 h. After washed with water, the obtained sample was denoted as Ru-$MoO_2$@PC/rGO.

In addition, Ru-$MoO_2$@PC/rGO (10 and 40), $MoO_2$@PC, and Ru-$MoO_2$@PC were obtained from $RuCl_3$-NENU-5/GO (10 and 40 mg), NENU-5 and Ru-NENU-5 through the similar way to Ru-$MoO_2$@PC/rGO, respectively.

**Instruments.** The structural and morphological features of the as-synthesized nanomaterials were analyzed by scanning electron microscope (JSM-7600F, JEOL), transmission electron microscopy (JEOL-2100F, JEOL), powder X-Ray diffraction (D/max 2500VL/PC, Japan), gas sorption analyzer (ASAP 2050, Micromeritics), X-ray photon spectroscopy (PHI 5000 Verasa Probe, ULAC-PHI), respectively.

**Electrochemical measurements.** The electrocatalytic HER properties were investigated in a typical three-electrode setup on a CHI 760E in 1.0 M KOH solution. 4 mg of the designed catalyst and 60 μL of nafion solution (5 wt%) were uniformly dispersed in 1940 μL of ethanol by continuously sonicating for at least 30 min. Subsequently, 5 μL of the ink was decorated on a glassy carbon electrode (GCE, 0.14 mg $cm^{-2}$). For comparison, commercial Pt/C (20 wt%) catalyst was also prepared with the same method. An Hg/HgO and graphite rod were utilized as the reference and counter electrode, respectively. Noticeably, the Hg/HgO electrode was calibrated in $H_2$-saturated 1.0 M KOH solution, where the Pt foil was used as the working and counter electrode, respectively (Fig. S20, EIS†). $E_{RHE} = 0.924\ V + E_{Hg/HgO}$.

Additionally, cyclic voltammetry (CV) at a sweep rate of 100 mV $s^{-1}$ and linear sweep voltammetry (LSV) at 5 mV $s^{-1}$ were carried out, respectively. In this work, the potentials were corrected with 95% iR drop compensation. The double-layer capacitor ($C_{dl}$) was assessed using CVs at 20-100 mV $s^{-1}$ in the region of 24-124 mV.

To investigate the stability at a large current density, the obtained catalyst was also loaded on carbon cloth (1*1 $cm^{-2}$, loading amount:1 mg $cm^{-2}$).

**Computational Details**

Density functional theory (DFT) calculations have been carried out using the Vienna ab-initio simulation package (VASP). The Perdew-Burke-Ernzerbof (PBE) exchange and correlation functional is chosen.[1, 2] To describe the interactions between valence electrons and ion cores, the Blöchl's all-electron-like projector augmented wave (PAW) method is used.[3, 4] The plane wave basis set kinetic cutoff energy of 450 eV with a Monkhost-Pack k-point grid of 3×3×1 are

applied.[5] The convergence tolerance of total energy calculation is determined at $1.0 \times 10^{-6}$ eV/atom with ionic force minimization level of 0.01 eV/Å. A vacuum layer as large as 20 Å is used along the c direction to avoid the periodic interactions.

The Gibbs free energies for HER are calculated by utilizing the computational hydrogen electrode model[6, 7]:

$$\Delta G = \Delta E + \Delta ZPE - T\Delta S \qquad (1)$$

Where $\Delta E$ is the energy difference of adsorption. $\Delta ZPE$ and $T\Delta S$ are the zero-point energy correction term and the entropy correction term, respectively. The two terms are obtained by the frequency calculation at T=300 K.[8] The Gibbs free energy of $(H^+ + e^-)$ is equivalent to the energy of 1/2 $G_{H2}$ in the study.

**References**


(1) J. P. Perdew, K. Burke, M. Ernzerhof, *Phys. Rev. Lett.* 1996, **77**, 3865-3868.

(2) G. Kresse, J. Hafner, *Phys. Rev. B* 1993, **47**, 558-561.

(3) P. E. Blöchl, *Phys. Rev. B* 1994, **50**, 17953-17979.

(4) G. Kresse, D. Joubert, *Phys. Rev. B* 1999, **59**, 1758-1775.

(5) H. J. Monkhorst, J. D. Pack, *Phys. Rev. B* 1976, **13**, 5188-5192.

(6) J. K. Nørskov, J. Rossmeisl, A. Logadottir, L. Lindqvist, *J. Phys. Chem. B* 2004, **108**, 17886-17892.

(7) Y. Jiao, Y. Zheng, M. Jaroniec, S. Z. Qiao, *J. Am. Chem. Soc.* 2014, **136**, 4394-4403.

(8) B. Delley, *J. Chem. Phys.* 1990, **92**, 508.

## S1. Figures in Supporting Information

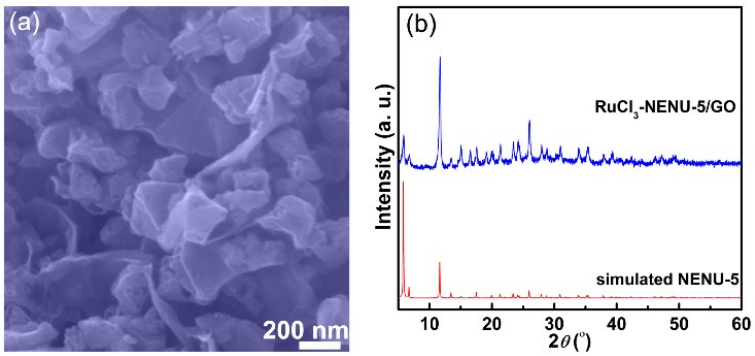


**Fig. S1** (a) SEM image and (b) PXRD pattern of $RuCl_3$-NENU-5/GO.

In Fig. S1a, the SEM image displays that the obtained $RuCl_3$-NENU-5 crystals with the octahedral or slightly truncated octahedral morphology, are homogeneously decorated over the GO nanosheets. The PXRD measurement was performed to examine the phase structure of $RuCl_3$-NENU-5/GO. In Fig. S1b, the PXRD pattern of $RuCl_3$-NENU-5/GO coincides well with simulated NENU-5, supporting that the crystal structures preserve nearly intact. Hence, these results significantly highlight the feasibility of this synthetic route.

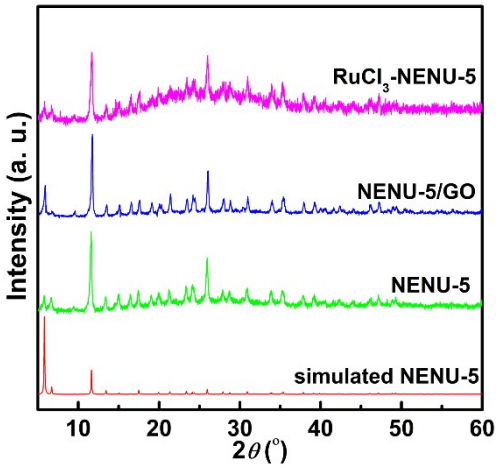


**Fig. S2** PXRD patterns of simulated NENU-5, as-synthesized NENU-5, NENU-5/GO, and $RuCl_3$-NENU-5, respectively.

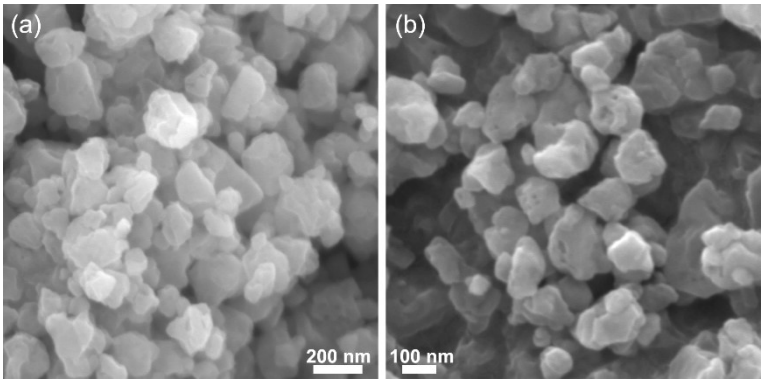


**Fig. S3** (a, b) SEM images of NENU-5.

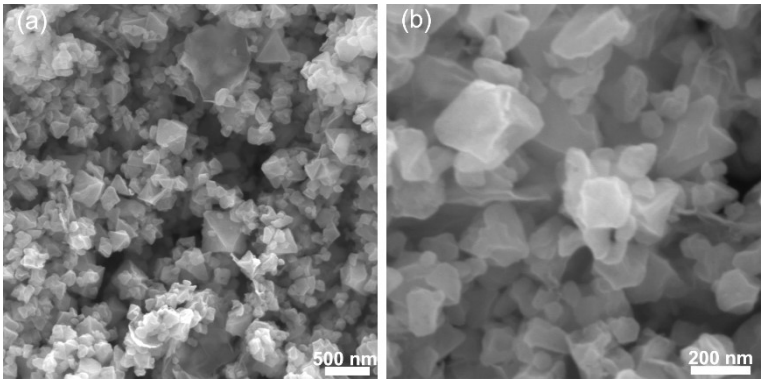


**Fig. S4** (a, b) SEM images of NENU-5/GO.

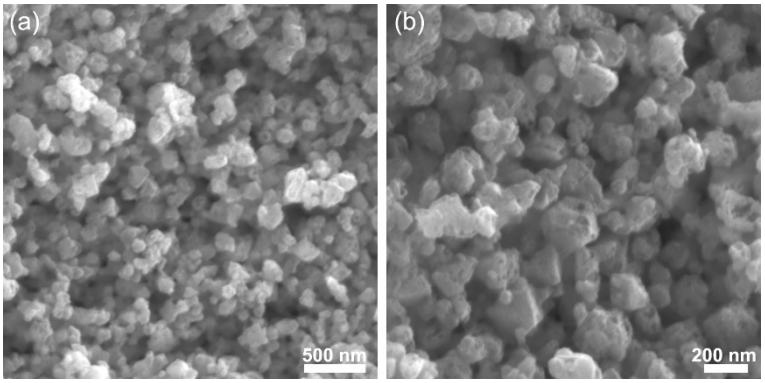


**Fig. S5** (a, b) SEM images of $RuCl_3$-NENU-5.

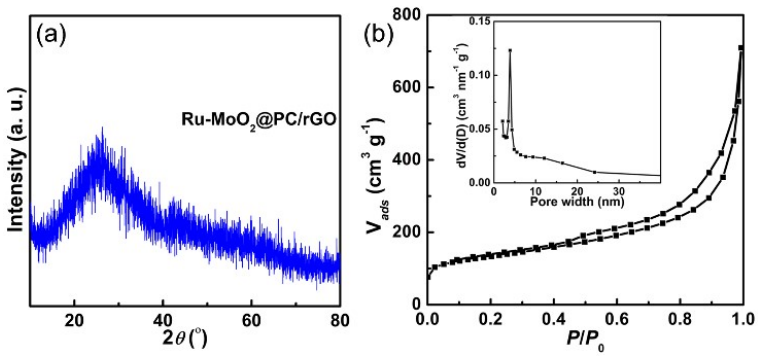


**Fig. S6** (a) PXRD pattern and (b) $N_2$ sorption isotherm of Ru-$MoO_2$@PC/rGO. Inset of (b) is the corresponding pore size distribution.

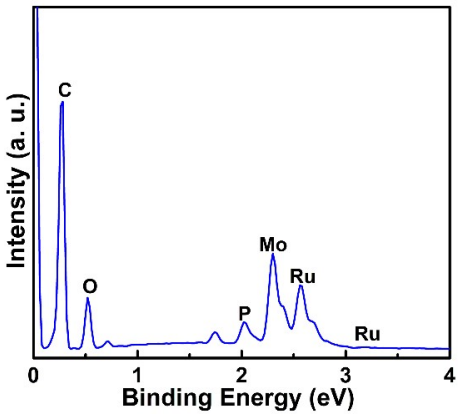


**Fig. S7** EDS of Ru-$MoO_2$@PC/rGO.

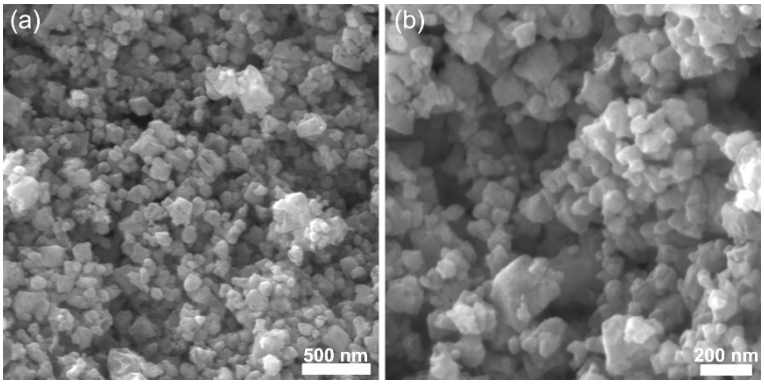


**Fig. S8** (a, b) SEM images of $MoO_2$@PC.

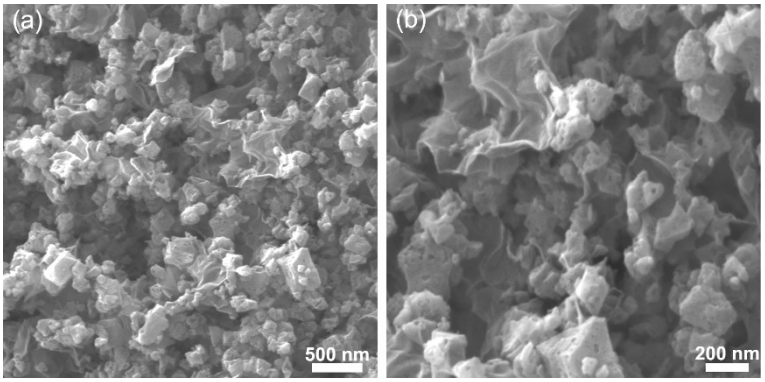


**Fig. S9** (a, b) SEM images of $MoO_2$@PC/rGO.

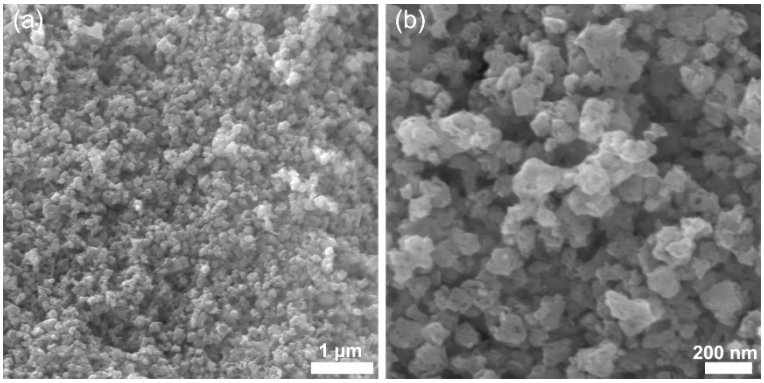


**Fig. S10** (a, b) SEM images of Ru-$MoO_2$@PC.

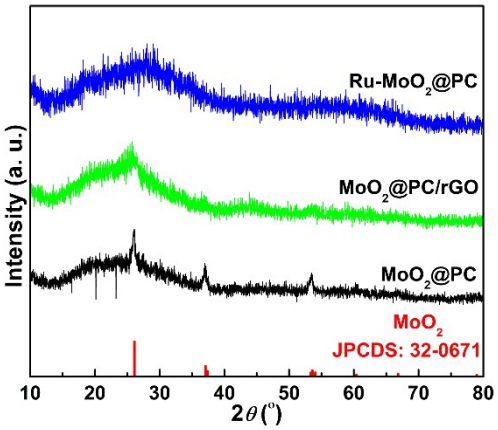


**Fig. S11** PXRD patterns of $MoO_2$@PC, $MoO_2$@PC/rGO, and Ru-$MoO_2$@PC, respectively.

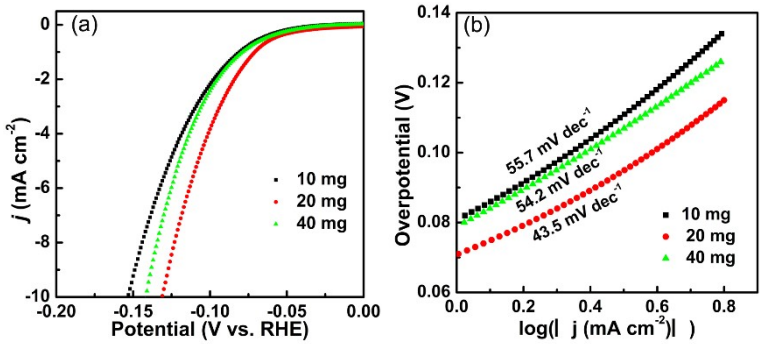


**Fig. S12** (a) Polarization curves and (b) Tafel plots of Ru-$MoO_2$@PC/rGO with different loadings of rGO (10, 20, and 40 mg).

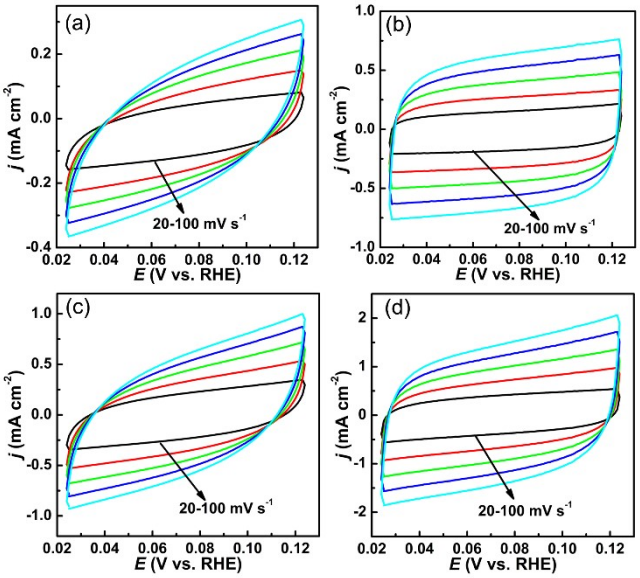


**Fig. S13** (a-d) CV curves of $MoO_2$@PC, $MoO_2$@PC/rGO, Ru-$MoO_2$@PC, and Ru-$MoO_2$@PC/rGO measured within the range of 24-124 mV vs. RHE with scan rate from 20 to 100 mV $s^{-1}$, respectively.

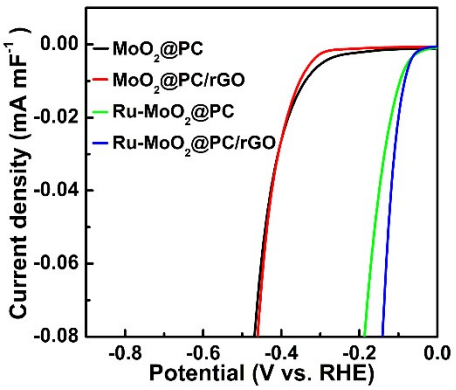


**Fig. S14** Normalized HER activities of different catalysts.

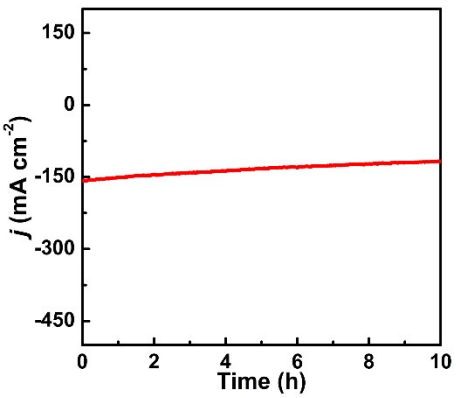


**Fig. S15** Chronopotentiometry curves of Ru-$MoO_2$@PC/rGO at 150 mA $cm^{-2}$.

As shown in Fig. S15, 80.6% of the current density could be remained during continuously operating at 150 mA $cm^{-2}$ for 10 h.

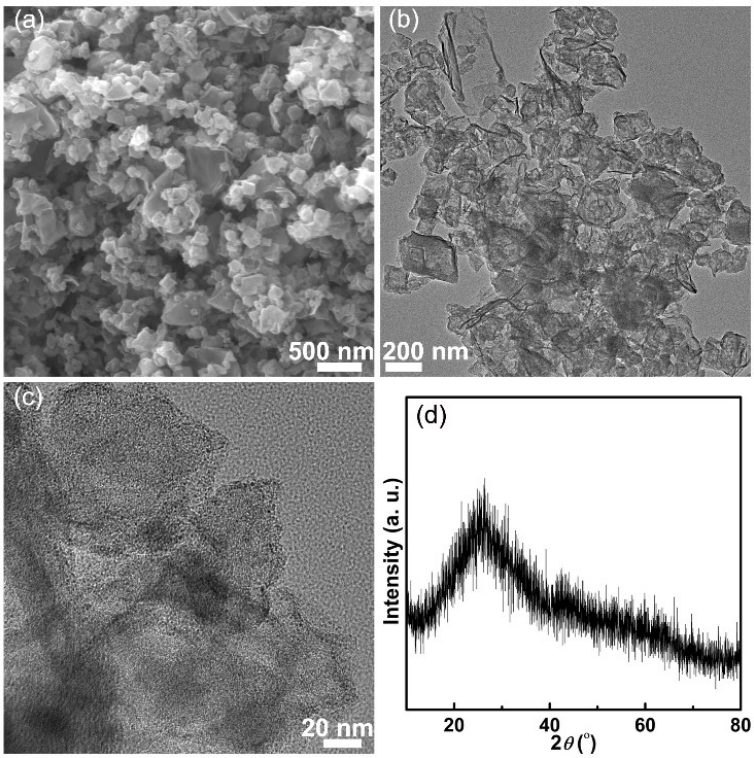


**Fig. S16** (a) SEM, (b, c) TEM images, and (d) PXRD of Ru-$MoO_2$@PC/rGO after stability test.

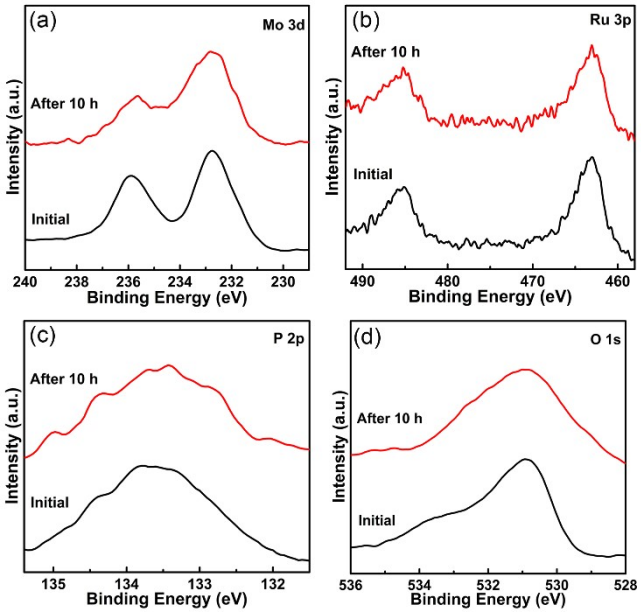


**Fig. S17** (a-d) High-resolution spectra of Mo 3d, Ru 3p, P 2p, and O 1s of Ru-$MoO_2$@PC/rGO, after HER stability test.

"As shown in Fig. S17, the XPS analysis proves that the chemical states remain unchanged after durability tests. The contents of C, Mo, Ru, P, and O are 73.8, 2.75, 2.37, 0.62, and 20.46 at%, respectively."

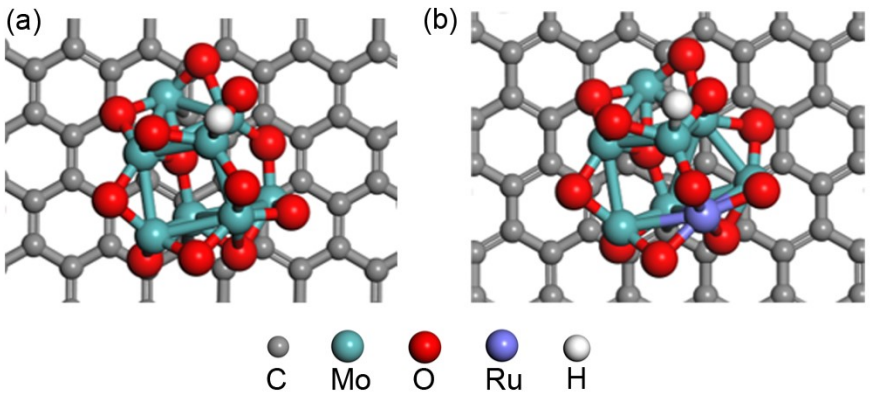


**Fig. S18** (a, b) Top views of $MoO_2$@PC/rGO and Ru-$MoO_2$@PC/rGO after optimization, where the Mo atoms are substituted by Ru atoms on the Ru-$MoO_2$@PC/rGO.

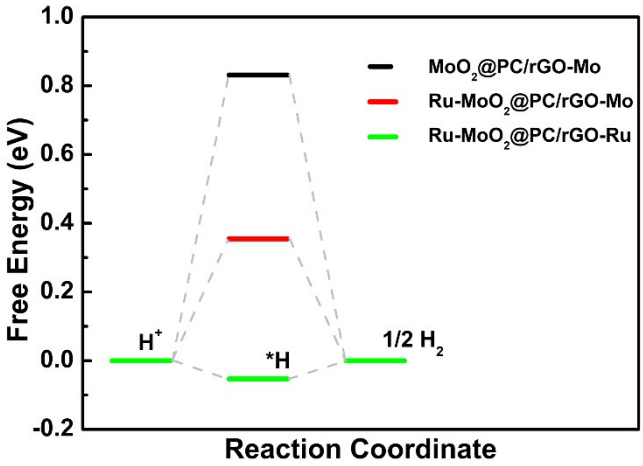


**Fig. S19** Free energy diagram on single-sites of $MoO_2$@PC/rGO and Ru-$MoO_2$@PC/rGO for HER.

"DFT calculations were performed to fundamentally comprehend into the remarkable HER performance of Ru-$MoO_2$@PC/rGO. As the first step of DFT calculations, we propose two rational models with three possible sites named as $MoO_2$@PC/rGO-Mo, Ru-$MoO_2$@PC/rGO-Mo, and Ru-$MoO_2$@PC/rGO-Ru (Fig. S18). As is well known, the HER activity is strongly related to the Gibbs free energy of hydrogen adsorption ($\Delta G^*_H$) on the catalysts surface. As shown in Fig. S19, the $\Delta G^*_H$ for Ru-$MoO_2$@PC/rGO-Ru, Ru-$MoO_2$@PC/rGO-Mo, and $MoO_2$@PC/rGO-Mo is -0.0534, 0.355, and 0.833 eV, respectively. The $|\Delta G^*_H|$ value of Ru-$MoO_2$@PC/rGO-Ru closest

to zero implies the excellent behavior to adsorb hydrogen. On the basis of DFT calculations, the introduction of Ru atoms on the $MoO_2$@PC/rGO surface can accelerate electron transfer in the catalytic process, and Ru-doping in the Mo site may boost electrocatalytic process by offering numerous active sites for HER, which significantly explains why Ru-$MoO_2$@PC/rGO shows outstanding HER activity."

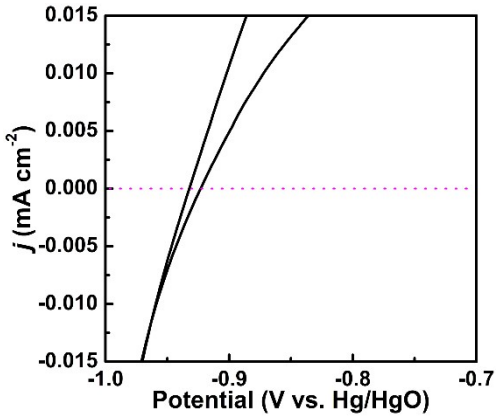


**Fig. S20** Single cycle CV curves of Hg/HgO electrode calibration in 1.0 M KOH.

## S2. Table in Supporting Information

**Table S1**. Comparison of catalytic performance of Ru-$MoO_2$@PC/rGO and other reported materials toward HER in in alkaline conditions.

| Catalysts | Tafel slope [mV $dec^{-1}$] | $\eta_{10}$ (mV) | References |
|---|---|---|---|
| **Ru-$MoO_2$@PC/rGO** | **43.5** | **126** | **This work** |
| $(Ni_xFe_{1-x})_2P$@PC/PG | 45 | 242 | *Adv. Funct. Mater.* 2021, 31, 2010912. |
| $MoO_2/MoS_2$/C | 49 | 91 | *Adv. Funct. Mater.* 2021, 31, 2101715. |
| CoP@FeCoP/NC | 56.34 | 141 | *Chem. Eng. J.* 2021, 403, 126312. |
| Ru/$Co_4N$-$CoF_2$ | 144 | 53 | *Chem. Eng. J.* 2021, 414, 128865. |
| S-$CoO_x$/NF | 80 | 136 | *Nano Energy* 2020, 71, 104652. |
| FeCo/$Co_2P$@NPCF | 120 | 260 | *Adv. Energy Mater.* 2020, 10, 1903854. |
| $MoO_2$-FeP@C | 48 | 103 | *Adv. Mater.* 2020, 32, 2000455. |
| Mo-$Ni_3S_2/Ni_xP_y$/NF | 68.4 | 109 | *Adv. Energy Mater.* 2020, 10, 1903891 |
| NiFeP@C | 75.8 | 160 | *ACS Appl. Mater. Interfaces* 2020, 12, 19447. |
| Cr-doped FeNiP/NCN | 69.5 | 190 | *Adv. Mater.* 2019, 31, 1900178. |
| NiFeP/NCH | 125 | 216 | *J. Am. Chem. Soc.* 2019, 141, 7906. |
| Fe-CoP | 92 | 78 | *Adv. Sci.* 2018, 5, 1800949. |
| CoP@BCN | 52 | 215 | *Adv. Energy Mater.* 2017, *7*, 1601671. |

## S3. Note in Supporting Information

**Note 1.** The HER process in alkaline media can be described using the following elementary steps：

under alkaline condition:

$$H_2O + e^- \rightarrow H_{ads} + OH^- \qquad \text{(Volmer reaction)}$$

$$H_{ads} + H_2O + e^- \rightarrow H_2 + OH^- \qquad \text{(Heyrovsky reaction)}$$